RSC Advances

PAPER

View Article Online
View Journal | View Issue

Cite this: *RSC Adv.*, 2024, **14**, 1944

Opposite regulation effects of Al^{3+} on different types of carbon quantum dots and potential applications in information encryption

Changdao Han,†[a] Huan Yang,†[b] Yan Fan,[a] Zhikun Wang,[a] Pei Li, *[b] Jie Jiang,[b] Mohan Huang,[a] Jing Xu, *[a] Junlang Chen *[a] and Liang Chen [b]

Received 15th November 2023
Accepted 1st January 2024

DOI: 10.1039/d3ra07801a

rsc.li/rsc-advances

Regulating the photoluminescence (PL) of carbon quantum dots (CQDs) through ion modification is a well-established and effective approach. Herein, we report the opposite regulation effects of Al^{3+} ions on the PL properties of two distinct types of CQDs (graphene quantum dots, GQDs, and nitrogen-doped carbon quantum dots of 2,3-diaminophenazine, DAP), and elucidate the underlying mechanism of the binding of Al^{3+} ions to different PL sites on CQDs by employing ultraviolet-visible spectroscopy, X-ray photoelectron spectroscopy, and density functional theory calculations. Specifically, Al^{3+} ions are primarily situated around the oxygen-containing groups, which do not impact the π–π regions of GQDs. However, Al^{3+} ions are preferentially adsorbed on the top of pyridine nitrogen in the phenazine rings of DAP, thus reducing the PL regions of DAP. Based on the opposite PL effects of Al^{3+} on GQDs and DAP, we explore potential applications of information encryption and successfully realize multi-level information encryption and decryption, which may provide new strategies for CQDs in information security.

1. Introduction

Quantum dots (QDs) are nanoscale semiconductor materials with unique optical properties, such as high brightness, narrow emission spectra, and tunable emission wavelengths,[1] which have attracted wide attention in the fields of optoelectronic devices,[2,3] energy storage,[4,5] biosensing[6,7] and biomedicine.[8,9] Among many types of QDs, carbon quantum dots (CQDs) are a new type of zero-dimensional carbon nanomaterial[10–12] with unique optical properties, such as tunable photoluminescence (PL), good biocompatibility, low toxicity and easy preparation.[13,14] Due to their excellent PL performance,[15] CQDs have attracted extensive attention in various fields, such as chemical sensing,[16,17] fluorescence imaging,[18,19] tumor diagnostics,[20,21] anti-counterfeiting[22] and information security.[23] However, the PL mechanism of CQDs is still not fully understood,[24] and the factors that affect their PL properties are complex and diverse.[25–28] Therefore, exploring the PL regulation of CQDs is of great significance for understanding their PL mechanism and expanding their application potential.

Among these methods, the surface modification of CQDs with metal ions is a simple and effective approach.[29] Metal ions can interact with the surface of CQDs through electrostatic interactions[30,31] or ligand effects,[16,30,32] thereby altering CQDs' charge states, energy level structures,[33] and surface morphology,[34] thus influencing their PL properties. In general, certain heavy metal ions can cause fluorescence quenching of CQDs, since their cation–π interactions with CQDs lead to the disruption of π–π bonds in CQDs. For example, Barman *et al.* prepared graphitic carbon nitride quantum dots (g-CNQD, a nitrogen-doped CQDs) using microwave mediated method. They found that the selective affinity of Hg^{2+} to g-CNQDs caused the fluorescence quenching of g-CNQDs,[35] and realized the "ON–OFF–ON" fluorescence response of g-CNQDs with the help of Hg^{2+} and I^-. Wang *et al.* first reported the fluorescence quenching of CQDs by Fe^{3+}, enabling the concentration detection of Fe^{3+}.[36] Shen *et al.* have also reported the synthesis of new nitrogen and sulfur co-doped graphene quantum dots (N,S-GQDs) and their application as fluorescence probes for the parallel and specific detection of Fe^{3+}, Cu^{2+}, and Ag^+, based on the aggregation-induced-quenching of N,S-GQDs.[37] Further, Li *et al.* confirmed that metal ions (such as Fe^{3+}, Cr^{3+}, and Cu^{2+}) were adsorbed on the center of the aromatic rings of CQDs, leading to the decrease of π-conjugation regions and as a result, quenching the fluorescence of CQDs.[38] On the other hand, metal ions may be able to restore or enhance the fluorescence of some specific CQDs. For example, As^{3+} ions can enhance the fluorescence emission of magnetic Fe-GQDs due to the restricted intramolecular rotations induced by the unusual Fe-GQDs–As^{3+} interactions.[39] Similarly, Zn^{2+}-passivated carbon dots (CDs) can restore the fluorescence of CDs synthesized from

[a]*Department of Optical Engineering, College of Optical, Mechanical and Electrical Engineering, Zhejiang A&F University, Hangzhou 311300, China. E-mail: chenjunlang7955@sina.com; jingxu@zafu.edu.cn*

[b]*School of Physical Science and Technology, Ningbo University, Ningbo 315211, China. E-mail: lipei@nbu.edu.cn*

† These authors contributed equally to this work.

glucose. Zn^{2+} prevented uncontrolled condensation and aggregation during pyrolysis, while acting as a surface passivator, helping to stabilize CDs and further enhance PL strength.[40] Fu *et al.* prepared CDs using one-step electrolysis methods for the selective detection of Al^{3+}. In contrast to the fluorescence quenching of GQDs by Fe^{3+} and Cr^{3+}, Al^{3+} may chelate with the abundant oxygen functional groups on the surface of the CDs, which increases the rigidity of the CDs and leads to enhanced fluorescence.[41]

However, studies on the different regulatory effects of metal ions on different CQDs have not been complete. Therefore, it is still a very important direction to further research the ion-mediated control of the PL of CQDs. Such investigations hold the potential to expand the application scenarios of CQDs in various fields, such as biomedical imaging, sensor technology, and information security. In this work, we investigated the PL effects of Al^{3+} on two types of CQDs, namely graphene quantum dots (GQDs) and nitrogen-doped carbon quantum dots (2,3-diaminophenazine, DAP). Specifically, Al^{3+} either maintains or slightly enhances the fluorescence of GQDs, yet it quenches the fluorescence of DAP. To elucidate the mechanism underlying the distinct effects of Al^{3+}, ultraviolet-visible absorption spectroscopy (UV-vis), X-ray photoelectron spectroscopy (XPS), and density-functional theory (DFT) calculations were employed. Based on the PL effects of Al^{3+} on GQDs and DAP, we propose an application of multi-level information encryption, which may pave a new technical route for information security.

2. Materials and methods

2.1 Materials

Starch, anhydrous ethanol, $FeCl_3$, and $AlCl_3$ were purchased from Shanghai Aladdin Biochemical Technology Co., Ltd (China). 2,3-Diaminophenazine (DAP, 95%) was obtained from Shanghai Dingfen Chemical Technology Co. Aqueous chloride solutions of various salts were prepared with deionized water of 18.2 MΩ resistivity. The thin-layer silica gel (GF254) plates were purchased from Zhejiang Taizhou Luqiao Sijia Biochemical Plastic Factory (China). All reagents were utilized directly without purification.

2.2 Synthesis of CQDs

We selected GQDs and DAP as two kinds of CQDs because both GQDs and DAP are electronegative, but the difference lies in that the electronegativity of GQDs originates primarily from oxygen-containing groups, whereas that of DAP derives from pyridine nitrogen atoms. GQDs were prepared from soluble starch by an eco-friendly hydrothermal synthesis method.[42] The detailed steps were as follows: 0.12 g soluble starch was first dissolved in 100 mL of deionized water and the mixture was stirred at 60 °C for 15 min, then the solution was transferred into a PTFE-lined stainless-steel autoclave and further heated at 190 °C for 2 h. After the reaction was completed, it was centrifuged for 30 min and then filtered through a 0.22 μm MCE membrane to remove the impurities such as sediment. Finally, the GQDs solution with a concentration of 2.5 mg mL^{-1} was obtained by proportional dilution. DAP was dissolved in anhydrous ethanol to obtain a 5 μg mL^{-1} solution.

2.3 Characterization

Fluorescence photographs were acquired by a UV analyzer (ZF-7N, Shanghai Jiapeng Technology Co., Ltd) under UV light irradiation at 365 nm and 254 nm. Fluorescence spectra were recorded by a fluorescence spectrometer (F-4600, Hong Kong Tianmei Co., Ltd), with the slit widths of 0.5 nm for all measurements. All UV-vis spectra were performed at room temperature by a UV-vis/NIR spectrophotometer (UH4150, Hitachi High-Tech Science Corporation, Japan) in the wavelength range of 200–800 nm. The samples were freeze-dried using a gland vacuum freeze dryer (LGJ-10, Beijing Songyuan Huaxing Co., Ltd). XPS was carried out by Thermo Scientific K-Alpha spectrometer, with an excitation source of Al Kα rays ($h\nu$ = 1486.60 eV), and the charge correction and data processing were performed using Avantage 5.9931 software with an energy standard of C1s at 284.80 eV. Transmission electron microscopy (TEM) images of GQDs were measured by JEM-2100F microscope.

2.4 Theoretical calculation

Theoretical calculations were conducted using the Gaussian 16 program package,[43] and all structural optimization and frequency calculations were performed at the M06-2X[44]/Def2-SVP,[45] level of theory. All optimized structures exhibited positive frequencies. The adsorption energies (ΔE) were calculated using the following equation:

$$\Delta E = E(Al^{3+}@M) - E(M) - E(Al^{3+})$$

where $E(Al^{3+}@M)$ represents the total energy of the Al^{3+} cation adsorbed on the substrate material model. $E(M)$ is the energy of the substrate material. $E(Al^{3+})$ denotes the energy of the Al^{3+} cation.

2.5 Fluorescence intensity detection

In a typical experiment, 1.6 mL of 2.5 mg mL^{-1} aqueous solution of GQDs and 1.6 mL of 5 μg mL^{-1} anhydrous ethanol solution of DAP were separately mixed with 1.6 mL of $AlCl_3$ solution with the concentrations varying from 0.1 mM to 10 mM. The fluorescence quenching and enhancement were assessed by the relative fluorescence ratio (F/F_0), where F and F_0 denote the fluorescence intensity of GQDs and DAP before and after the addition of ions, respectively. The fluorescence brightness of these solutions was examined under UV light irradiation (center wavelength 365 nm) and captured by photographs.

3. Results and discussion

3.1 Opposite PL effects of Al^{3+} on GQDs and DAP

We first measured the size distribution of GQDs in water. Fig. 1a and b show that GQDs are well dispersed in water, and the particle size of GQDs ranges from 0.5 to 2.5 nm, with the highest

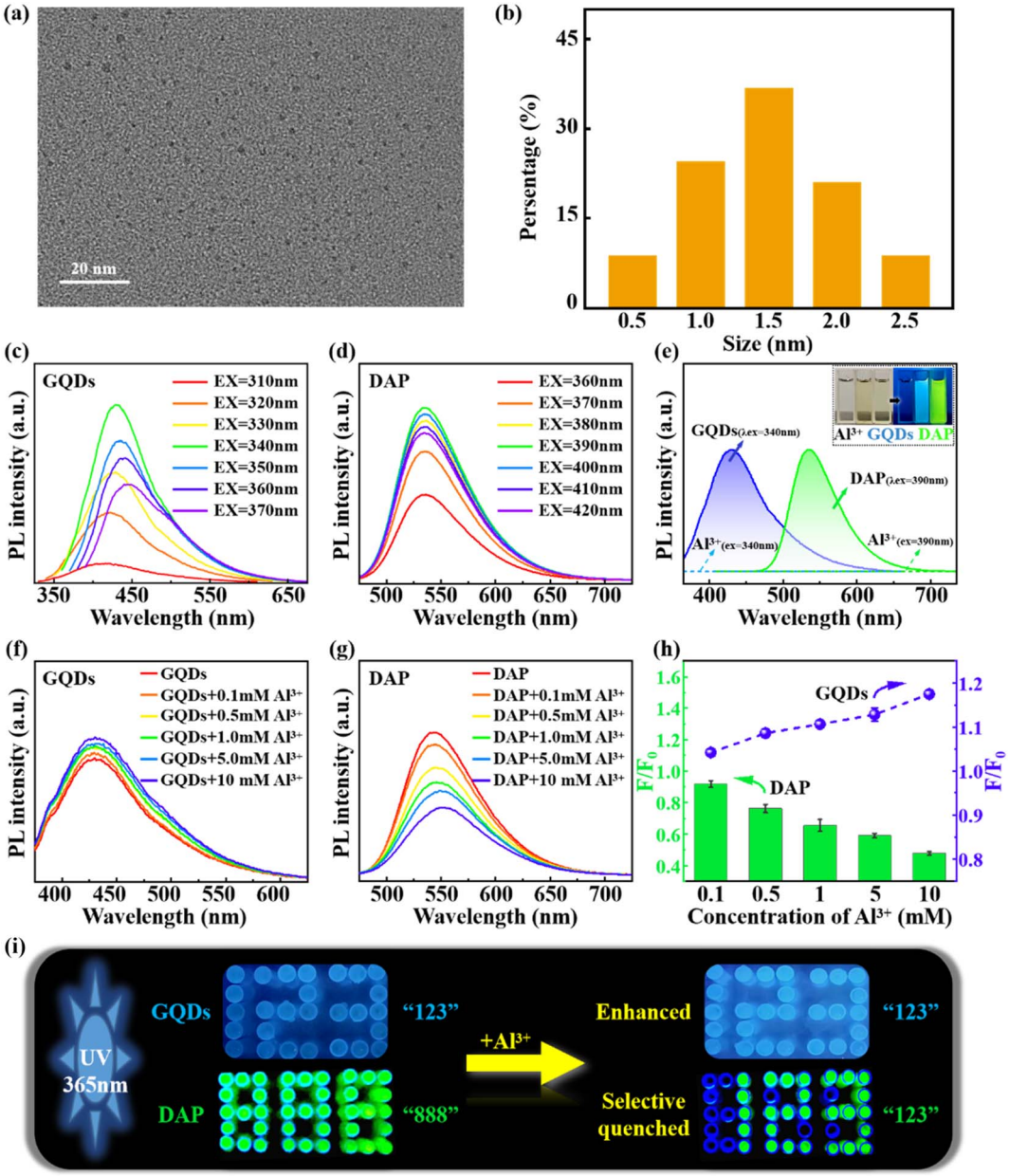

Fig. 1 (a) TEM image of GQDs. (b) Size distribution of GQDs. Fluorescence emission spectra of GQDs (c) and DAP (d) at excitation wavelengths of 310–370 nm for GQDs and 360–420 nm for DAP. (e) Fluorescence emission spectra of $AlCl_3$ (340 nm and 390 nm), GQDs (340 nm) and DAP (390 nm) solutions. The inset illustrates the $AlCl_3$, GQDs and DAP solutions under natural and UV lights. Fluorescence emission spectra of GQDs (f) and DAP (g) with the increasing concentrations of Al^{3+} from 0.1 to 10 mM. (h) Relative fluorescence intensity of (f) and (g). (i) Photographs of fluorescence enhancement of GQDs and quenching of DAP by Al^{3+}.

frequency around 1.5 nm. We used fluorescence spectra of GQDs and DAP without Al^{3+} as control, at the excitation wavelengths of 310–370 nm for GQDs, and 360–420 nm for DAP. As shown in Fig. 1c and d, both GQDs and DAP have PL properties. Meanwhile, we observed that the optimal excitation wavelengths of GQDs and DAP were 340 nm and 390 nm, respectively. Therefore, these two UV wavelengths were employed in the following PL experiments. Fig. 1e shows the colour of $AlCl_3$, GQDs and DAP solutions under natural and UV lights. It has been found that the $AlCl_3$ solution has no fluorescence under natural and UV lights, indicating that Al^{3+} and Cl^- themselves have no PL properties. Similarly, GQDs and DAP have no fluorescence under natural light. In contrast, GQDs emit blue fluorescence and DAP glows with green fluorescence under UV lights.

Then, we explored the effects of Al^{3+} on the PL properties of GQDs and DAP. $AlCl_3$ solution was added into GQDs and DAP (denoted as Al^{3+}@GQDs and Al^{3+}@DAP) with concentrations ranging from 0.1 to 10 mM. The mixtures were irradiated by UV lights with their respective optimal excitation wavelengths. The fluorescence intensities of pure GQDs and DAP were also measured as controls. Interestingly, we observed that the

fluorescence intensities of GQDs were gradually enhanced with the increasing concentration of Al^{3+} (Fig. 1f), while those of DAP were gradually weakened (Fig. 1g). Fig. 1h shows that the relative fluorescence intensity of GQDs increases from 1.0 to 1.2, while that of DAP decreases from 1.0 to 0.5 with the increasing Al^{3+} concentrations from 0 to 10 mM, which implies that Al^{3+} has opposite effects on the PL properties of different CQDs.

Fig. 1i illustrates the opposite regulation of Al^{3+} on the PL of GQDs and DAP, in which each pixel point is the top view of a cuvette filled with GQDs or DAP. We observed that the fluorescence intensity of the number "123" emitted from GQDs was obviously enhanced by the addition of Al^{3+}. On the contrary, the green fluorescence of the number "888" emitted from DAP was selectively quenched by the addition of Al^{3+}, and the unquenched fluorescence of cuvettes that are not added with Al^{3+} shows the number "123", which confirms again the opposite regulation of the PL of different CQDs by Al^{3+}.

We performed UV-vis spectra to reveal the mechanism of the opposite regulation effects of Al^{3+} on the PL of different CQDs. As shown in Fig. 2a, the UV-vis spectra of both pure GQDs and Al^{3+}@GQDs exhibit absorption peaks at 227 nm and 282 nm,[42] corresponding to the π–π* transitions of C=C and C–C, and n–π* transitions induced by defects or oxygen-containing groups in GQDs,[46,47] respectively. The absorption peaks of Al^{3+}@GQDs are slightly higher than those of GQDs at both positions, and generally rise with the increasing Al^{3+} concentrations, indicating that the presence of Al^{3+} facilitates the electron transitions of GQDs. In other words, Al^{3+} ions bind to the defects or oxygen-containing groups of the GQDs through weak electrostatic or coordination interactions, thereby influencing the charge transfer of GQDs.[13,48] Consequently, the adsorption of Al^{3+} on GQDs does not impair the main π-conjugated PL regions of GQDs, which does not lead to the fluorescence quenching of GQDs.

Similarly, the UV-vis spectra of pure DAP and Al^{3+}@DAP (Fig. 2b) also show two absorption peaks near 260 nm and 435 nm,[49,50] respectively. The two peaks are separately designated to the π–π* transitions of C=C/C=N and electron transitions in the conjugate structure between the phenazine rings and $-NH_2$ groups of DAP.[49,51] On the contrary, the intensity of the absorption peaks of Al^{3+}@DAP at the π–π* transition is significantly lower than that of pure DAP, and the two absorption peaks are red-shifted, which may be attributed to the interactions of Al^{3+} with the phenazine rings and the $-NH_2$ groups.[47,52] In other words, Al^{3+} is most likely adsorbed on the π-conjugated regions of DAP, resulting in the diminution of the π-conjugated regions, and thus weakening the fluorescence of DAP, contrary to the fluorescence enhancement of Al^{3+} on GQDs.

Furthermore, the regulation mechanism of Al^{3+} on the PL of GQDs and DAP was analysed by XPS spectra. As shown in Fig. 3a–c, the survey spectra illustrate that the GQDs are mainly composed of 286.12 eV of C1s and 533.01 eV of O1s, with an atomic content percentage of C : O = 65.65 : 34.35. Then, the C1s spectrum shows four peaks at 284.8, 286.4, 287.7, and 288.5 eV, with an error margin of ±0.2 eV in both GQDs and Al^{3+}@GQDs, corresponding to C–C/C=C, C–O–C/C–OH, C=O, and O=C–OH,[16,49] implying that GQDs and Al^{3+}@GQDs still have the same chemical composition. However, the addition of Al^{3+} has a greater effect on the oxygen-containing groups of GQDs and relatively enhances the PL of GQDs dominated by π-conjugated regions, which is consistent with the results of UV-vis spectra. The high-resolution spectrum of the O1s further indicates that the C=O groups of GQDs are more affected by Al^{3+}, compared with the C–O chemical sites.[49,53]

As shown in Fig. 3d–f, the survey spectra of DAP consist mainly of 285.41 eV of C1s and 399.43 eV of N1s, with an atomic content percentage of C : N ≈ 3 : 1. Similarly, the C1s spectrum exhibits four peaks at 284.8, 286.0 and 288.7 eV, with an error margin of ±0.3 eV in both DAP and Al^{3+}@DAP, corresponding to C–C/C=C, C–N and NH_2 groups,[16] respectively. These overlapped peaks indicate that pure DAP and Al^{3+}@DAP still have the same chemical composition, yet their intensity varies about the π-conjugated regions of the phenazine ring of DAP, especially pyridine nitrogen, which may lead to the attenuation of the PL of DAP. The high-resolution spectrum of the N1s of DAP shows that the pyridine nitrogen in the phenazine ring of DAP is more affected by the Al^{3+} than that near the $-NH_2$ groups at the edge of DAP[54] in agreement with the results of UV-vis spectra.

To gain molecular-level insights into the adsorption of Al^{3+} on the two types of CQDs, quantum chemical calculations were performed for Al^{3+}@GQDs and Al^{3+}@DAP complexes. We employed the $C_{54}H_{18}$ hydrocarbon as the model for GQDs and the $C_{46}N_8H_{18}$ hydrocarbon as the model for DAP with the same

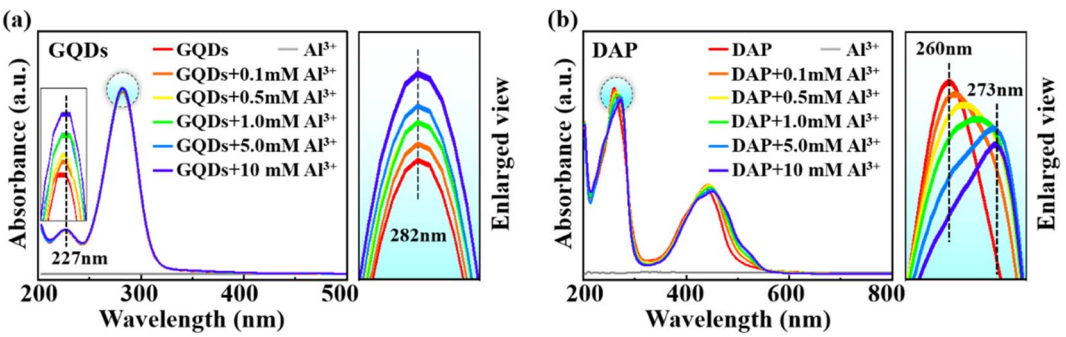

Fig. 2 UV-vis spectra of GQDs (a) and DAP (b) with and without Al^{3+}. The right panels are magnifications of the specified regions (highlighted by circles).

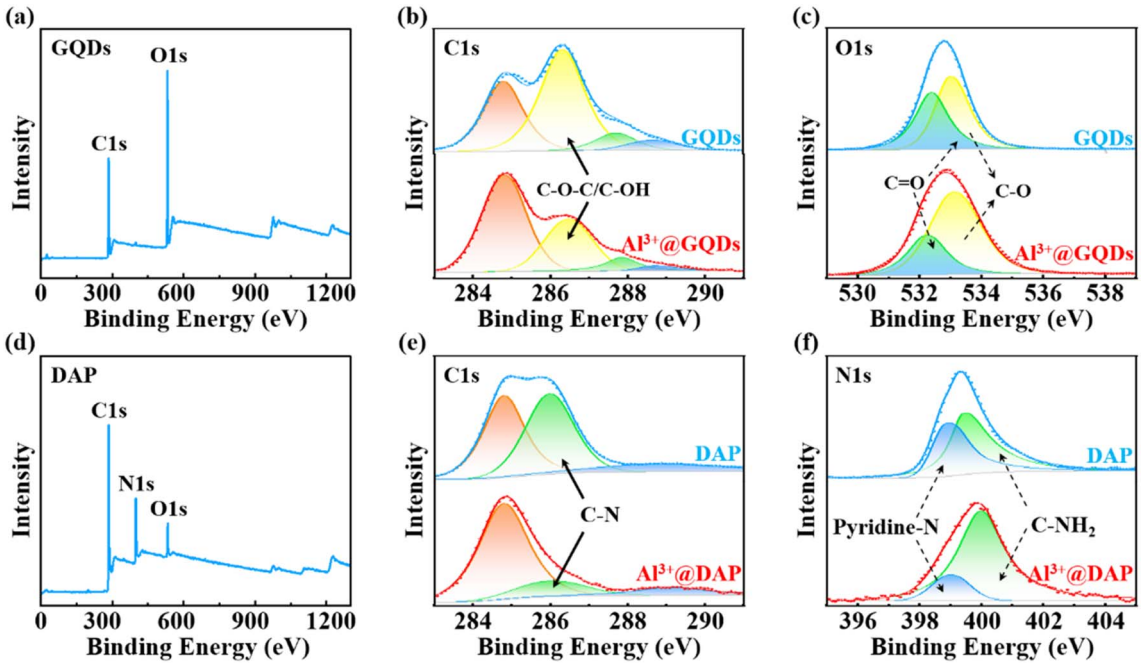

Fig. 3 (a)–(c) XPS spectra of GQDs and Al^{3+}@GQDs and fine spectra of C1s and O1s. (d)–(f) XPS spectra of DAP and Al^{3+}@DAP and fine spectra of C1s and N1s.

molecular size as GQDs to compare their adsorption energies against Al^{3+}. The calculated results have demonstrated the stable adsorption of Al^{3+} on both models, as shown in Fig. 4a and b. Specifically, in the Al^{3+}@GQDs complex, Al^{3+} adsorbs above the center of the benzene ring with an adsorption height of 2.52 Å. In contrast, in the Al^{3+}@DAP complex, Al^{3+} adsorbs on the top of a nitrogen atom with an adsorption height of 2.25 Å. Additionally, due to the strong interaction between nitrogen and the cation, the planar structure is slightly distorted to expose the nitrogen atom to the surface. As depicted in Fig. 4c, the calculated adsorption energies, energies corrected with zero-point energy, and Gibbs free energies for Al^{3+}@DAP are approximately 770 kcal mol^{-1}. In comparison, the corresponding values for Al^{3+}@GQDs are around 650 kcal mol^{-1}. These results indicate that DAP exhibits a stronger adsorption capacity for Al^{3+} than GQDs.

It has been reported that heavy metal ions (such as Fe^{3+}) can cause fluorescence quenching of CQDs, due to their strong cation-π interactions with the aromatic rings of CQDs, which inhibit the π–π* transitions of the aromatic rings.[55,56] Interestingly, we found that Al^{3+} can restore the PL of GQDs that are quenched by Fe^{3+}. As shown in Fig. 5a, when 0.8 mL of 0.1 mM Fe^{3+} was added to the GQDs, the relative fluorescence ratio of Fe^{3+}@GQDs was reduced to 0.92, exhibiting a fluorescence quenching effect. However, the relative fluorescence ratio of Fe^{3+}@Al^{3+}@GQDs increased and recovered to 1.00 when 0.8 mL of 1.0 mM Al^{3+} was added. And with the increasing Al^{3+} concentration, the fluorescence intensity of Fe^{3+}@Al^{3+}@GQDs continued to enhance, which confirmed again that the binding site of Al^{3+} is not on the centre of the aromatic rings of GQDs, but near the defects or oxygen-containing groups of GQDs. Conversely, when Fe^{3+} and Al^{3+} were added to DAP, the relative

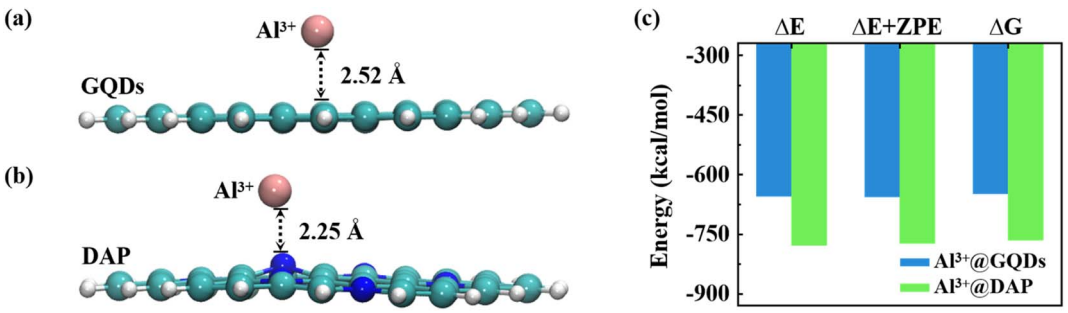

Fig. 4 (a) and (b) The most stable geometries of Al^{3+}@GQDs and Al^{3+}@DAP complexes. Spheres in green, white, and blue denote carbon, hydrogen, and nitrogen atoms, respectively. Pink balls represent Al^{3+} cations. Adsorption distances (in Å) are listed. (c) The calculated adsorption energies, zero-point corrected energies, and Gibbs free energies of Al^{3+}@GQDs and Al^{3+}@DAP at the level of M06-2X/Def2-SVP.

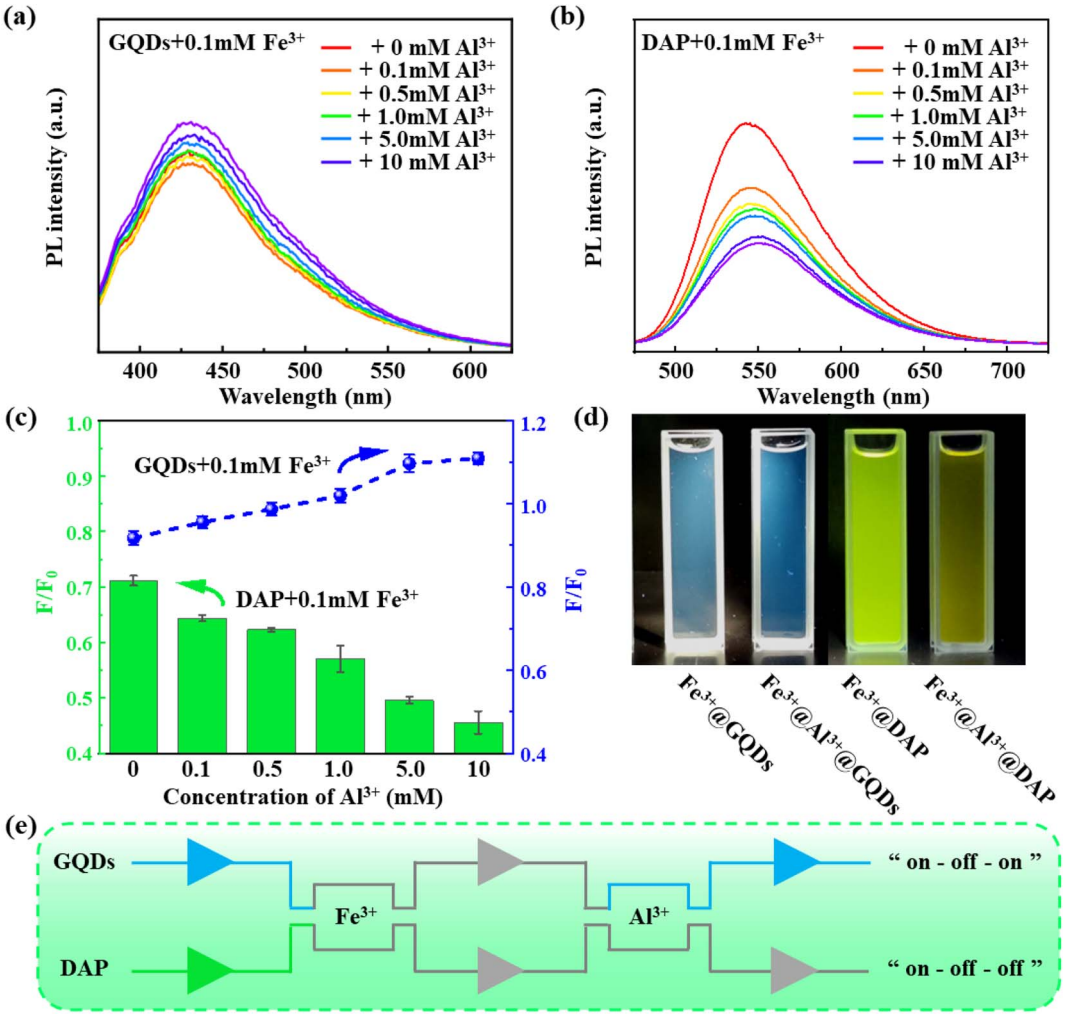

Fig. 5 Fluorescence emission spectra of (a) Fe^{3+}@Al^{3+}@GQDs and (b) Fe^{3+}@Al^{3+}@DAP. (c) Relative fluorescence intensity of Fe^{3+}@Al^{3+}@GQDs and Fe^{3+}@Al^{3+}@DAP. (d) Fluorescence pictures of Fe^{3+}@GQDs and Fe^{3+}@DAP before and after the addition of Al^{3+}. (e) Schematic illustration of fluorescence response of GQDs and DAP with Fe^{3+} and Al^{3+}.

fluorescence ratio of Fe^{3+}@Al^{3+}@GQDs was always lower than 1.0 (Fig. 5b and c), and no fluorescence restoration or enhancement effect was observed. This indicates that both Fe^{3+} and Al^{3+} tend to bind to the phenazine ring of DAP and inhibit its fluorescence emission. Fig. 5d demonstrated that the addition of Al^{3+} caused the fluorescence of Fe^{3+}@DAP to be significantly attenuated, while the fluorescence intensity of Fe^{3+}@GQDs was augmented. Fig. 5e shows the schematic illustration of the fluorescence response of GQDs and DAP with $Fe^{3+}$and Al^{3+}. The PL of GQDs can be quenched by Fe^{3+} and further restored by the addition of Al^{3+}. This process was termed as "on–off–on", which may be utilized to exploit fluorescence switch. As a comparison, the quenched PL of DAP by Fe^{3+} is further quenched by the addition of Al^{3+}, denoted as "on–off–off".

3.2 Potential applications in information encryption

Eventually, we devised special applications of multilevel information encryption using the opposite effects of Al^{3+} on GQDs and DAP. As shown in Fig. 6a, we wrote the letters "wo" and "man" on a card using $AlCl_3$ and Al^{3+}@GQDs solutions, respectively. After the card was dried, the handwriting vanished under natural light, effectively hiding the letters "wo" and "man" and implementing information encryption. Then, under the irradiation of UV light (365 nm), the letters "man" written by Al^{3+}@GQDs appear clearly, while the letters "wo" written by $AlCl_3$ solution are still invisible, since the $AlCl_3$ solution has no fluorescent effect, thus realizing the first level decryption. Finally, the DAP solution is sprayed on the card. Due to the fluorescence quenching effect of Al^{3+} on DAP, the dark trace of the letters "wo" emerges instead. On the other hand, the letters "man" written by Al^{3+}@GQDs can still emit weak fluorescence after being coated by the DAP solution. Thus, the word "woman" appears intact, achieving the second level decryption of information.

We designed another scheme of multi-level information encryption using ion regulation strategy, which is based on the different PL effects of Al^{3+} and Fe^{3+}. The detailed process was depicted in Fig. 6b, first, we wrote the equation "1949 + 74 = 2023" on a GF254 plate, in which "19|23" and "49 − 74 = 20"

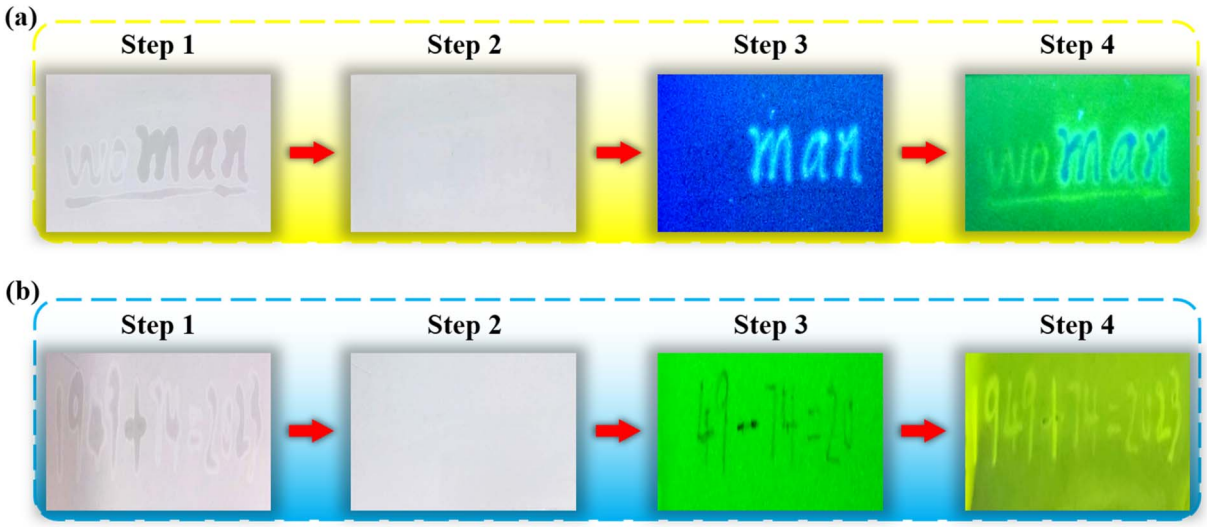

Fig. 6 (a) Multi-level information encryption and decryption scheme for GQDs and DAP by Al^{3+}. (b) Multi-level information encryption and decryption design strategies for other fluorescent carriers by metal ions.

were written by $AlCl_3$ and $FeCl_3$ solutions, respectively. After drying, the original handwriting disappeared under natural light, effectively concealing the information of "1949 + 74 = 2023" (step 2). Then, the card was exposed to the UV light (254 nm), and it emitted green fluorescence. However, the dark trace of "49 − 74 = 20" appeared, since Fe^{3+} has a fluorescence quenching effect on GF254. The rest of the equation "19|23" written by $AlCl_3$ solution is still invisible, since Al^{3+} has no fluorescence quenching effect on GF254, thus realizing the first-level decryption (step 3). Finally, DAP solution was sprayed on GF254. Because Al^{3+} can quench the fluorescence of DAP, the dark trace of "19|23" also appeared, and the whole equation "1949 + 74 = 2023" was unveiled, achieving the second-level information decryption.

4. Conclusion

In summary, we investigated the effects of Al^{3+} on the PL properties of two types of CQDs (GQDs and DAP), and found that Al^{3+} can exert opposite effects on different CQDs, namely, enhancing the fluorescence of GQDs whereas quenching the fluorescence of DAP. UV-vis spectra indicate that the PL of GQD and DAP are mainly attributed to the π–π* transitions of carbon atoms in the aromatic rings at 227 nm and the N-doped phenazine rings near 260 nm, respectively. XPS spectra further confirm that Al^{3+} ions are mainly located around the oxygen-containing groups, which does not affect the π–π regions of GQDs. However, XPS spectra and DFT calculations demonstrate that Al^{3+} ions prefer to be adsorbed on the top of pyridine nitrogen within the phenazine rings of DAP, thus reducing the PL regions of DAP. In addition, the PL of GQDs, which is quenched by Fe^{3+} and restored by Al^{3+}, exhibits an "on–off–on" fluorescence response. Based on these findings, we have proposed two strategies of information encryption, which may have potential application prospects in the future.

Author contributions

L. C. and J. C. conceived the ideas. L. C., J. C., C. H., J. X., and Y. F. designed the experiments, simulations and co-wrote the manuscript. C. H., H. Y., P. L., J. J., Y. F., Z. W., and M. H. performed the experiments and prepared the data graphs. J. X. performed the simulations. All authors discussed the results and commented on the manuscript.

Conflicts of interest

The authors declare no competing financial interests.

Acknowledgements

This work was supported by the National Natural Science Foundation of China (No. 12075211, 12074341, 11975206), the Scientific Research and Developed Funds of Ningbo University (No. ZX2022000015), and the Zhejiang Provincial Natural Science Foundation of China (No. LY22A040008).

References

1 V. I. Klimov, S. A. Ivanov, J. Nanda, M. Achermann, I. Bezel, J. A. McGuire and A. Piryatinski, *Nature*, 2007, **447**, 441–446.
2 D. Ghosh, K. Sarkar, P. Devi, K.-H. Kim and P. Kumar, *Renewable Sustainable Energy Rev.*, 2021, **135**, 110391.
3 X. Li, M. Rui, J. Song, Z. Shen and H. Zeng, *Adv. Funct. Mater.*, 2015, **25**, 4929–4947.
4 H. Lu, Z. Huang, M. S. Martinez, J. C. Johnson, J. M. Luther and M. C. Beard, *Energy Environ. Sci.*, 2020, **13**, 1347–1376.
5 J.-S. Wei, C. Ding, P. Zhang, H. Ding, X.-Q. Niu, Y.-Y. Ma, C. Li, Y.-G. Wang and H.-M. Xiong, *Adv. Mater.*, 2019, **31**, 1806197.

6 X. Liu, H. Jiang, J. Ye, C. Zhao, S. Gao, C. Wu, C. Li, J. Li and X. Wang, *Adv. Funct. Mater.*, 2016, **26**, 8694–8706.
7 L. Cui, X. Ren, J. Wang and M. Sun, *Mater. Today Nano*, 2020, **12**, 100091.
8 W. C. Chan and S. Nie, *Science*, 1998, **281**, 2016–2018.
9 C. Fu, L. Qiang, Q. Liang, X. Chen, L. Li, H. Liu, L. Tan, T. Liu, X. Ren and X. Meng, *RSC Adv.*, 2015, **5**, 46158–46162.
10 X. Xu, R. Ray, Y. Gu, H. J. Ploehn, L. Gearheart, K. Raker and W. A. Scrivens, *J. Am. Chem. Soc.*, 2004, **126**, 12736–12737.
11 Y.-P. Sun, B. Zhou, Y. Lin, W. Wang, K. A. S. Fernando, P. Pathak, M. J. Meziani, B. A. Harruff, X. Wang, H. Wang, P. G. Luo, H. Yang, M. E. Kose, B. Chen, L. M. Veca and S.-Y. Xie, *J. Am. Chem. Soc.*, 2006, **128**, 7756–7757.
12 Y. Wang, Y. Zhu, S. Yu and C. Jiang, *RSC Adv.*, 2017, **7**, 40973–40989.
13 S. Liu, J. Tian, L. Wang, Y. Zhang, X. Qin, Y. Luo, A. M. Asiri, A. O. Al-Youbi and X. Sun, *Adv. Mater.*, 2012, **24**, 2037–2041.
14 T. Liu, J. X. Dong, S. G. Liu, N. Li, S. M. Lin, Y. Z. Fan, J. L. Lei, H. Q. Luo and N. B. Li, *J. Hazard. Mater.*, 2017, **322**, 430–436.
15 C. Ding, A. Zhu and Y. Tian, *Acc. Chem. Res.*, 2014, **47**, 20–30.
16 Y. Fang, S. Guo, D. Li, C. Zhu, W. Ren, S. Dong and E. Wang, *ACS Nano*, 2012, **6**, 400–409.
17 M. M. Hussain, W. U. Khan, F. Ahmed, Y. Wei and H. Xiong, *Chem. Eng. J.*, 2023, **465**, 143010.
18 S. N. Baker and G. A. Baker, *Angew. Chem., Int. Ed.*, 2010, **49**, 6726–6744.
19 S. Zhu, Q. Meng, L. Wang, J. Zhang, Y. Song, H. Jin, K. Zhang, H. Sun, H. Wang and B. Yang, *Angew. Chem., Int. Ed.*, 2013, **52**, 3953–3957.
20 J. Yan, G. Pan, W. Lin, Z. Tang, J. Zhang, J. Li, W. Li, X. Lin, H. Luo and G. Yi, *Chem. Eng. J.*, 2023, **451**, 138922.
21 R. Wang, K.-Q. Lu, Z.-R. Tang and Y.-J. Xu, *J. Mater. Chem. A*, 2017, **5**, 3717–3734.
22 S. Y. Lim, W. Shen and Z. Gao, *Chem. Soc. Rev.*, 2014, **44**, 362–381.
23 N. Murugan, M. Prakash, M. Jayakumar, A. Sundaramurthy and A. K. Sundramoorthy, *Appl. Surf. Sci.*, 2019, **476**, 468–480.
24 S. Zhu, J. Zhang, X. Liu, B. Li, X. Wang, S. Tang, Q. Meng, Y. Li, C. Shi, R. Hu and B. Yang, *RSC Adv.*, 2012, **2**, 2717–2720.
25 A. P. Alivisatos, *Science*, 1996, **271**, 933–937.
26 W. L. Wilson, P. F. Szajowski and L. E. Brus, *Science*, 1993, **262**, 1242–1244.
27 E. H. Nicollian, *J. Vac. Sci. Technol.*, 1971, **8**, S39–S49.
28 J. Wang, C.-F. Wang and S. Chen, *Angew. Chem., Int. Ed.*, 2012, **51**, 9297–9301.
29 F. Li, C. Liu, J. Yang, Z. Wang, W. Liu and F. Tian, *RSC Adv.*, 2013, **4**, 3201–3205.
30 L. Cao, S.-T. Yang, X. Wang, P. G. Luo, J.-H. Liu, S. Sahu, Y. Liu and Y.-P. Sun, *Theranostics*, 2012, **2**, 295–301.
31 Y. Yang, J. Cui, M. Zheng, C. Hu, S. Tan, Y. Xiao, Q. Yang and Y. Liu, *Chem. Commun.*, 2011, **48**, 380–382.
32 B. Yin, J. Deng, X. Peng, Q. Long, J. Zhao, Q. Lu, Q. Chen, H. Li, H. Tang, Y. Zhang and S. Yao, *Analyst*, 2013, **138**, 6551–6557.
33 C. Fowley, N. Nomikou, A. P. McHale, B. McCaughan and J. F. Callan, *Chem. Commun.*, 2013, **49**, 8934–8936.
34 Y. Liu, C. Liu and Z. Zhang, *Appl. Surf. Sci.*, 2012, **263**, 481–485.
35 S. Barman and M. Sadhukhan, *J. Mater. Chem.*, 2012, **22**, 21832–21837.
36 D. Wang, L. Wang, X. Dong, Z. Shi and J. Jin, *Carbon*, 2012, **50**, 2147–2154.
37 C. Shen, S. Ge, Y. Pang, F. Xi, J. Liu, X. Dong and P. Chen, *J. Mater. Chem. B*, 2017, **5**, 6593–6600.
38 J. Li, Z. Wang, J. Yang, X. Xia, R. Yi, J. Jiang, W. Liu, J. Chen, L. Chen and J. Xu, *Appl. Surf. Sci.*, 2021, **546**, 149110.
39 S. Pathan, M. Jalal, S. Prasad and S. Bose, *J. Mater. Chem. A*, 2019, **7**, 8510–8520.
40 M. Yang, Q. Tang, Y. Meng, J. Liu, T. Feng, X. Zhao, S. Zhu, W. Yu and B. Yang, *Langmuir*, 2018, **34**, 7767–7775.
41 X.-C. Fu, J.-Z. Jin, J. Wu, J.-C. Jin and C.-G. Xie, *Anal. Methods*, 2017, **9**, 3941–3948.
42 J. Yang, P. Li, Z. Song, J. Li, H. Yang, F. Yan, L. Li, C. Xu, J. Chen and L. Chen, *Appl. Surf. Sci.*, 2022, **593**, 153367.
43 M. J. Frisch, G. W. Trucks, H. B. Schlegel, G. E. Scuseria, M. A. Robb, J. R. Cheeseman, G. Scalmani, V. Barone, B. Mennucci and G. Petersson, see also: URL: **http://www.gaussian.com**.
44 Y. Zhao and D. G. Truhlar, *Theor. Chem. Acc.*, 2008, **120**, 215–241.
45 D. Rappoport and F. Furche, *J. Chem. Phys.*, 2010, **133**, 134105.
46 S. Lu, L. Sui, J. Liu, S. Zhu, A. Chen, M. Jin and B. Yang, *Adv. Mater.*, 2017, **29**, 1603443.
47 H.-L. Yang, L.-F. Bai, Z.-R. Geng, H. Chen, L.-T. Xu, Y.-C. Xie, D.-J. Wang, H.-W. Gu and X.-M. Wang, *Mater. Today Adv.*, 2023, **18**, 100376.
48 W. Zhao, C. Song and P. E. Pehrsson, *J. Am. Chem. Soc.*, 2002, **124**, 12418–12419.
49 Q. Zhang, R. Wang, B. Feng, X. Zhong and K. Ostrikov, *Nat. Commun.*, 2021, **12**, 6856.
50 X. Tong, G. Cai, L. Xie, T. Wang, Y. Zhu, Y. Peng, C. Tong, S. Shi and Y. Guo, *Biosens. Bioelectron.*, 2023, **222**, 114981.
51 L. Cao, M. Zan, F. Chen, X. Kou, Y. Liu, P. Wang, Q. Mei, Z. Hou, W.-F. Dong and L. Li, *Carbon*, 2022, **194**, 42–51.
52 M. Lan, S. Zhao, Y. Xie, J. Zhao, L. Guo, G. Niu, Y. Li, H. Sun, H. Zhang, W. Liu, J. Zhang, P. Wang and W. Zhang, *ACS Appl. Mater. Interfaces*, 2017, **9**, 14590–14595.
53 H. S. Rady, M. H. Misbah and M. El-Kemary, *Carbon*, 2023, **214**, 118341.
54 H. Ding, S.-B. Yu, J.-S. Wei and H.-M. Xiong, *ACS Nano*, 2016, **10**(1), 484–491.
55 L. Chen, G. Shi, J. Shen, B. Peng, B. Zhang, Y. Wang, F. Bian, J. Wang, D. Li, Z. Qian, G. Xu, G. Liu, J. Zeng, L. Zhang, Y. Yang, G. Zhou, M. Wu, W. Jin, J. Li and H. Fang, *Nature*, 2017, **550**, 380–383.
56 F. Dai, F. Zhou, J. Chen, S. Liang, L. Chen and H. Fang, *J. Mater. Chem. A*, 2021, **9**, 10672–10677.